

Fluctuations and correlations during the shear flow of elastic particles near the jamming transition

Claus Heussinger, Pinaki Chaudhuri and Jean-Louis Barrat*

November 1, 2018

Abstract

We present a numerical study of the flow of an assembly of frictionless, soft discs at zero temperature, in the vicinity of and slightly above the jamming density. We find that some of the flow properties, such as the fluctuations in the number of contacts or the shear modulus, display a critical like behaviour that is governed by the proximity to the jamming point. Dynamical correlations during a quasistatic deformation, however, are non critical and dominated by system size. At finite strain rates, these dynamical correlations acquire a finite, strain-rate dependent amplitude, that decreases when approaching the jamming point from above.

Manuscript submitted to the themed Issue on granular and jammed materials of Soft Matter

1 Introduction and background

The properties of granular materials, in particular sand, are a constant source of fascination for children and adults alike, and are intrinsically related to the ability of such systems to exist in either solid or fluid states, under very similar conditions. For the scientist this fascination may arise through the apparent contradiction between the rigidity of the individual grains and the fragility of the assembly as a whole. This means that, for example, small changes in the loading conditions (such

as changing the inclination angle of the support) can lead to large scale structural rearrangements (“avalanches”) or even to the complete fluidization of the material. A few years ago, Liu and Nagel¹ have suggested a “phase-diagram” for this type of solid-liquid transition (“jamming”). At zero temperature the axes relate to the ways an unjamming transition can be triggered, either by increasing the external driving (e.g. shear stress) or by decreasing the density of the material. The present study will probe the vicinity of this “unjamming line” using quasistatic and finite strain rate simulations of a model granular system.

If one applies a shear stress, which is small and below a certain threshold (“yield-stress”), the material will respond as an elastic solid. Increasing the stress above the yield-stress, the particles will unjam and start to flow. This flow behavior is called “plastic flow” as the material will not revert to its original shape when the stress is removed.

In the following we will assume that the system can flow at arbitrary small strain-rates without showing flow-localization. That this is possible is by no means guaranteed, as in some instances co-existence of flowing and jammed states is observed.² We have not observed such a persistent strain localization in the simulations that are presented here.

Plastic flow is observed in a large number of glassy materials, that are a priori very different from the athermal granular systems close to point J (see below) studied in this paper. However, all materials display a rather universal behavior, that was illustrated already in early studies on the plastic-flow of metallic glasses.^{3,4} These studies have given indications that in the flowing phase the main plastic activity is spatially localized to so called shear transformation zones.^{5,6} These zones are non per-

*Université Lyon 1, Laboratoire de Physique de la Matière Condensée et Nanostructures, CNRS, UMR 5586 Domaine Scientifique de la Doua F-69622 Villeurbanne Cedex, France

sistent, localized in space, and presumably consist of a few atoms that undergo the irreversible rearrangements responsible for the observed plastic flow. Recently, this plasticity has been further analyzed in simulations with a focus on the quasistatic dynamics at small strain rates, close to the flow arrest.^{7–12} With these studies it was possible to trace back the origin of plastic activity to the softening of a vibrational mode and the vanishing of the associated frequency.⁷ In real space, this softening is associated with the formation of distinct, localized zones where the plastic failure is nucleated.⁸ In turn, this can trigger the failure of nearby zones, such that avalanches of plastic activity form that may “propagate” through the entire system.

It has been argued that the macroscopic extent of these avalanches is a signature of the quasistatic dynamics, which gives the system enough time to propagate the failure throughout the system. Beyond the quasistatic regime, i.e. farther away from the jammed state, the size of these events is expected to be finite. Thus, one naturally finds an increasing length-scale that is connected with the flow arrest upon reducing the stress towards the threshold value.^{13–15}

Without external drive, an (un)jamming transition can occur for decreasing particle volume fraction below a critical value, ϕ_c . This special point, which is only present in systems with purely repulsive steric interactions, has been given the name “point J”.^{16,17} At this point the average number of particle contacts jumps from a finite value z_0 to zero just below the transition. The value of z_0 is given by Maxwell’s estimate for the rigidity transition^{18,19} and signals the fact that at point J each particle has just enough contacts for a rigid/solid state to exist. This marginally rigid state is called “isostatic”. Compressing the system above its isostatic state a number of non-trivial scaling properties emerge.^{16,20} As the volume fraction is increased, additional contacts are generated according to $\delta z \sim \delta\phi^{1/2}$. The shear modulus scales as $G \sim p/\delta z$ and vanishes at the transition (unlike the bulk modulus).¹⁶ This scaling is seen to be a consequence of the non-affine deformation response of the system,²¹ with particles preferring to rotate around rather than to press into each other.²² Associated with the breakdown of rigidity at point J is the length-scale, $l^* \sim \delta z^{-1}$,^{23,24} which quantifies the size over which additional contacts stabilize the

marginally rigid isostatic state.

In this article we present results from quasistatic and small strain-rate flow simulations of a two-dimensional system in the vicinity of point J. Together with the linear elastic shear modulus, at point J also the yield-stress σ_y vanishes.^{25–30} Thus, point J is connected with a transition from plastic-flow behavior ($\phi > \phi_c$, $\sigma_y > 0$) to normal fluid flow ($\phi < \phi_c$, $\sigma_y = 0$), with either Newtonian²⁶ or Bagnold rheology^{27,29} at small strain-rates. In consequence, both (un)jamming mechanisms as described above are present at the same time: the flow arrest, as experienced by lowering the stress towards threshold, is combined with the vanishing of the threshold itself.

In this study we want to address two questions: In how far do the general plastic flow properties carry over to this situation of small or, indeed, vanishing yield-stress? Is the vicinity to point J and its isostatic state at all relevant for the flow properties? It will be shown that while the stress fluctuations reflect the critical properties at point J, dynamical correlations are typical those observed in the flow of elasto-plastic solids.

We will approach these questions starting with the quasistatic-flow regime. The advantage of quasistatic simulations is to provide a clean way of accessing the transition region between elastic, solid-like behavior and the onset of flow. In the quasistatic regime flow is generated by a succession of (force-)equilibrated solid states. Thus, one can connect a liquid-like flow with the ensemble of solid states that are visited along the trajectory through phase-space.

In Section 3.1, we study the instantaneous statistical properties of the configurations generated by this flow trajectory at zero strain rate, and show that they display large fluctuations in several quantities, that are associated with the proximity to the jamming point.

In Section 3.2, we follow the analysis of recent experiments³¹ and use a “four point correlation” tool to define a dynamical correlation length that characterizes the extension of the dynamical heterogeneities observed in the flow process. This dynamical length scale is shown to scale as the system size in the zero strain rate limit, independently of the distance to point J. The heterogeneity in the system is maximal for strains that correspond to the typical duration between the plastic avalanches

described above.

We complement this analysis with preliminary results from dissipative molecular-dynamics simulations that access strain-rates above the quasistatic regime. This allows us to assess the importance of dynamic effects in limiting access to certain regions of the landscape. Indeed, the results at larger strain rate are system size independent, and reveal a surprising growth of the strength of the heterogeneities with increasing packing fraction away from ϕ_c .

2 Simulations

Our system consists of N soft spherical particles with harmonic contact interactions

$$E(r) = k(r - r_c)^2. \quad (1)$$

Two particles, having radii r_i and r_j , only interact, when they are “in contact”, i.e. when their distance r is less than the interaction diameter $r_c = r_i + r_j$. This system has been studied in several contexts, for example in.^{16,26,32} The mixture consists of two types of particles (50 : 50) with radii $r_1 = 0.5d$ and $r_2 = 0.7d$ in two-dimensions. Three different system-sizes have been simulated with $N = 900$, 1600 and 2500 particles, respectively. The unit of length is the diameter, d , of the smaller particle, the unit of energy is kd^2 , where k is the spring constant of the interaction potential. We use quasistatic shear simulation, and compare some of the results with those obtained from dissipative molecular-dynamics simulations at zero temperature.

Quasistatic simulations consists of successively applying small steps of shear followed by a minimization of the total potential energy. The shear is implemented with Lee-Edwards boundary conditions with an elementary strain step of $\Delta\gamma = 5 \cdot 10^{-5}$. After each change in boundary conditions the particles are moved affinely to define the starting configuration for the minimization, which is performed using conjugate gradient techniques.³³ The minimization is stopped when the nearest energy minimum is found. Thus, as the energy landscape evolves under shear the system always remains at a local energy minimum, characterized by a potential energy, a pressure p and a shear stress σ .

The molecular dynamics simulations were performed by integrating Newton’s equations of motion with elastic forces as deduced from Eq. (1) and dissipative forces

$$\vec{F}_{ij} = -b[(\vec{v}_i - \vec{v}_j) \cdot \hat{r}_{ij}] \hat{r}_{ij}, \quad (2)$$

proportional to the velocity differences along the direction \hat{r}_{ij} that connects the particle pair. The damping coefficient is chosen to be $b = 1$. Rough boundaries are used during the shear, the boundaries being built by freezing some particles at the extreme ends in the y -direction, from a quenched liquid configuration at a given ϕ . The system is sheared by driving one of the walls at a fixed velocity in the x direction, using periodic boundary conditions in this direction.

For all system sizes, the distance between the top and bottom boundaries is $52.8d$ and each of the boundaries has a thickness of $4.2d$. The system size is changed by modifying the length of the box in the x -direction.

3 Results

3.1 Quasistatic simulations

As is readily apparent from Fig. 1, a typical feature of quasistatic stress-strain relations is the interplay of “elastic branches” and “plastic events”. During elastic branches stress grows linearly with strain and the response is reversible. In plastic events the stress drops rapidly and energy is dissipated.

In setting the elementary strain step, $\Delta\gamma$, care must be taken to properly resolve these events. Too large strain steps would make the simulations miss certain relaxation events. We chose a strain step small enough, such that most minimization steps do not involve any plastic relaxations. In consequence, the elastic branches are well resolved, each consisting of many individual strain steps.

The succession of elastic and plastic events defines the flow of the material just above its yield-stress $\sigma_y(\phi)$. The value of the yield-stress depends on volume-fraction and nominally vanishes at ϕ_c (see Fig. 2). For finite systems, however, finite-size effects dominate close to ϕ_c such that one cannot observe a clear vanishing of σ_y . Rather, as Fig. 1 shows, one enters an intermittent regime, i.e. a finite interval in volume-fraction in which the stress-

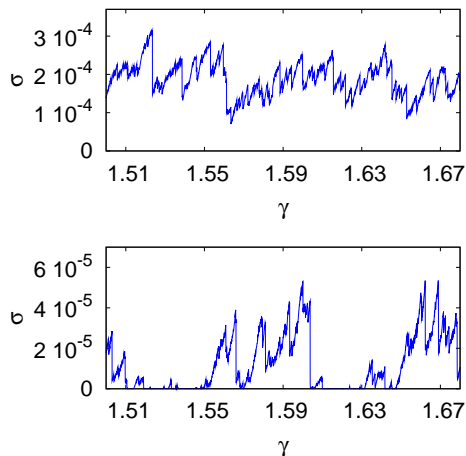


Figure 1: Stress-strain relation for two different volume-fractions, $\phi = 0.847$ (top) and $\phi = \phi_c = 0.8433$ (bottom). At volume-fractions close to ϕ_c the signal is intermittent showing long quiet regions where the system flows without the building up of stress.

signal shows a coexistence between jammed and “freely-flowing” states. This is evidence of a distribution of jamming thresholds, $P(\phi_c)$, which sharpens with increasing the system-size.^{16,28} A finite-size scaling analysis of this distribution allows one to extract the critical volume-fraction. To this end we count the number of jamming events that lead from the freely-flowing state to the jammed state and back¹. We find a maximum number of events at a certain $\phi_c(L)$, which can be extrapolated to $L = \infty$ to define the critical volume fraction of our simulation. The value we find, $\phi_c = 0.8433$ is slightly higher than what has been obtained previously, however, evidence is mounting that ϕ_c is non-universal³⁵ and depends on the details of the ensemble preparation. Scaling properties in the vicinity of a jamming threshold, on the other hand, appear to be universal.³⁵

In Fig. 2 we display the yield-stress σ_y , as a function of volume-fraction, $\delta\phi = \phi - \phi_c$, and pressure p . Finite-size effects are particularly strong when using ϕ as control variable. In the intermittent regime the average stress levels off to a system-size dependent value.

¹For a closer illustration of a jamming event see the supporting material to our previous paper³⁴

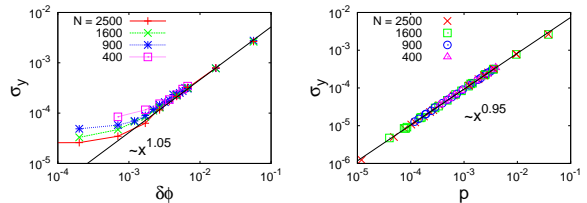


Figure 2: Average yield-stress as function of volume-fraction (left) and pressure (right). The yield-stress is determined as an average over stress-values just before plastic events occur, i.e. at the top end of each elastic branch.

Much better scaling behavior can be obtained, when using pressure as control variable, as this is characterized by the same finite-size effects as the shear-stress. In the following we will therefore use pressure as control variable. Be aware, however, that we do *not* run pressure-controlled simulations, as for example Peyneau and Roux²⁵ but use the average pressure, $\langle p \rangle(\phi)$, only to plot our simulation results. The value $\sigma/p \approx 0.1$ obtained from Fig. 2 is consistent with these pressure-controlled simulations. On the other hand, the scaling with volume-fraction, $p \sim \delta\phi^{1.1}$, is slightly stronger than in linear elasticity at zero stress,^{16,20} where the pressure simply scales as $\delta\phi$. In view of the strong finite-size effects, the scaling with volume-fraction should, however, be taken with care.

In the following we show results from five different volume-fractions, $\phi = 0.846, 0.848, 0.85, 0.86$ and $\phi = 0.9$, which are all above ϕ_c and *outside* the intermittent regime (i.e. no freely-flowing zero-stress states occur). For each volume-fraction we study three different system sizes with $N = 900, 1600$ and 2500 particles.

3.1.1 Elastic properties

As reviewed in the introduction a hallmark of the elasticity of solids in the vicinity of point J is the scaling of the linear elastic shear modulus $g \sim p^{1/2}$. Similarly, the number of inter-particle contacts scale as $z = z_0 + Ap^{1/2}$.

We have analyzed the elastic branches in the steady-state flow to find (Figs. 3 and 4) that the same scaling properties characterize the average nonlinear elastic modulus g_{avg} , which we define as

the local slope of the stress-strain curve, and also the associated contact numbers z_{avg} . If we take these scaling properties as a signature of the criticality of point J, we can conclude that for the range of volume-fractions considered we are in the “critical regime”.

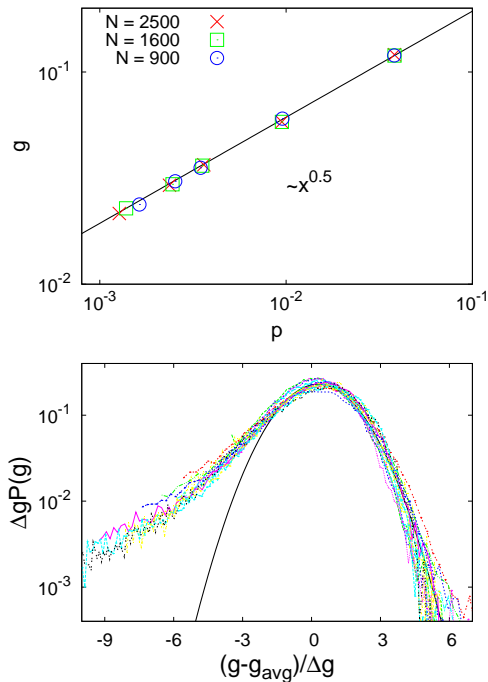


Figure 3: (Top) Average nonlinear elastic shear modulus g_{avg} as function of pressure p . (Bottom) Probability distribution $P(g)$ centered around average value g_{avg} and rescaled width according to $\Delta g = p^{0.25}/N^{0.5}$. Black solid line is a Gaussian pdf.

As additional characterization of the ensemble of elastic states we report the probability distributions of shear moduli and contact numbers, respectively. Maybe surprisingly all the obtained distributions have approximately the same shape and can be superimposed on a single master curve. To achieve this we center each distribution around the average value and rescale the width with a factor $p^\alpha N^\beta$.

By looking carefully at the individual distributions we do observe a slight trend towards the development of non-Gaussian tails close to ϕ_c . While non-Gaussian distributions are to be expected close

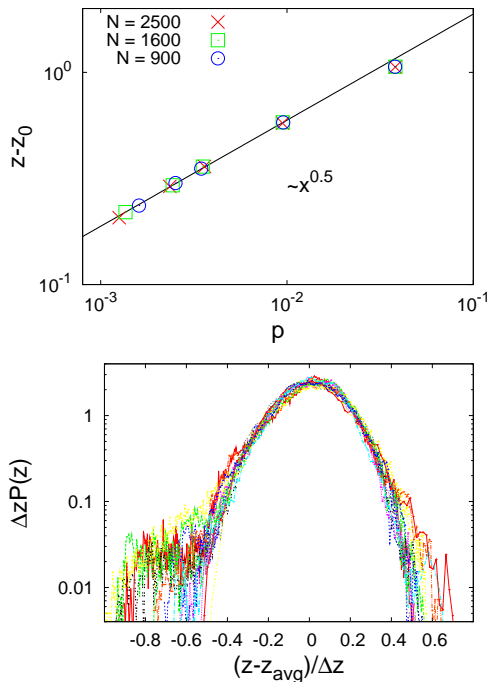


Figure 4: (Top) Average contact number z as function of pressure p . The values for $z_0 \equiv z(p=0)$ are determined from a best fit. They are smaller than $z_c = 4$ as to the presence of rattlers, which have not been accounted for. (Bottom) Probability distribution $P(z)$ centered around average value z_{avg} and rescaled width according to $\Delta z = p^{-0.35}/N^{0.5}$

to critical points,³⁶ the effect is quite small and all distributions have a well developed Gaussian core. The pronounced small- g tail of $P(g)$ is due to shear moduli that extend down to zero. Similar tails have been observed in⁸ and related to a softening of the response upon approach towards plastic instabilities. Indeed, we found that manually suppressing states close to plastic events, the weight in the small- g tail is reduced.

For the width of the g -distribution we obtain $\Delta g = p^{0.25}/N^{0.5}$. Thus, the absolute width of the distribution decreases with decreasing pressure, while the relative width, $\Delta g/g_{\text{avg}}$ diverges at point J. For the contact numbers, on the other hand, we find a divergence of the absolute width itself, $\Delta z = p^{-0.35}/N^{0.5}$. These enhanced fluctuations certainly support the view of δz as an order pa-

parameter for a continuous jamming transition. The quantity $\Delta z^2 N$ would then be analogous to a susceptibility, $\chi \sim p^{-\gamma}$, diverging with an exponent $\gamma = 0.7$.

Our results are different than those of Henkes and Chakraborty,³⁷ where fluctuations of z are found to be independent of pressure, $\Delta z \sim p^0$. Note, however, the subtle difference in ensemble. These authors study a pressure-ensemble, in which states are generated by quenching *random* particle configurations to the local minimum of the potential energy landscape (similar to the procedure in Ref.¹⁶). One may view these states as the inherent structures of a high temperature liquid. Our ensemble then corresponds to the inherent structures of a driven glassy material. We fix volume-fraction and sample only states that are connected by the trajectory of the system in phase-space. The ensemble therefore reflects the dynamics of the system and the region of phase-space where it is guided to.

3.1.2 Yield properties

We now go beyond the properties of the elastic states and discuss aspects related to their failure during the plastic events. As indicated in the introduction, plastic events can be viewed as bifurcations in energy-landscape. A local energy minimum vanishes and the system has to search for a new minimum at lower energy and stress. In quasistatic dynamics this process is instantaneous. The associated stress-drop is therefore visible as a vertical line in the stress-strain relation (Fig. 1).

In the following we characterize the amount of dissipation during a plastic event by the associated stress-drop, $\Delta\sigma$. The frequency of plastic events is discussed in terms of the length of elastic branches, $\Delta\gamma_{\text{avg}}$.

Just like the probability distributions within the elastic states, the functions $P(\Delta\sigma)$ and $P(\Delta\gamma_{\text{avg}})$ (Figs. 5 and 6) are universal and can be rescaled on a single master-curve. Here, it is sufficient to use the first moment of the distribution, i.e. the ensemble-averaged stress drops and elastic-branch lengths, respectively. As the logarithmic scale in the inset in Fig. 5 shows, the collapse for the stress-drop distribution is quite good for large as well as for small stress drops. The black line represents a fit of the form $\Delta\sigma^{-1} \exp(-\Delta\sigma/\sigma_L)$ with the stress-scale $\sigma_L \approx 5\Delta\sigma_{\text{avg}}$. The intermediate

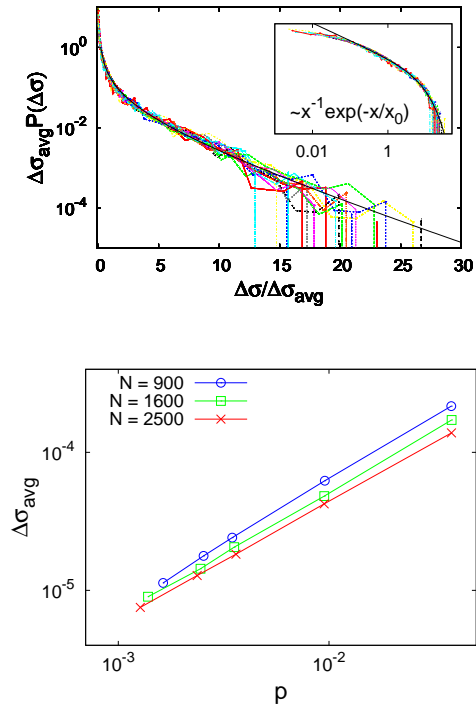


Figure 5: (Top) Distribution of stress-drops normalized with average values $\Delta\sigma_{\text{avg}}$. Inset shows the same figure in a log-log representation. (Bottom) Scaling of $\Delta\sigma_{\text{avg}}$ with pressure p .

power-law behaviour $P \sim \Delta\sigma^{-1}$ reflects the lack of scale related to a typical event size. The only relevant scale is the exponential cut-off at σ_L . Tewari *et al.*³⁸ have reported an exponent of -0.7 in the energy-drop distribution at finite-strain rates. The simulated systems are somewhat smaller, however. Kabla *et al.*³⁹ have found an exponent of -1.5 in a vertex model for foams, in agreement with renormalization group arguments.⁴⁰

The exponential tail has been observed in several different studies^{8,11,11,41,42} in two and in three spatial dimensions. Tsamados *et al.*¹¹ have furthermore related this feature of the stress-drop distribution to the diversity of local flow-defects causing the plastic event.

A similar universality has been observed by Maloney and Lemaitre.⁸ Their simulations are conducted with three different interaction potentials but without changing the density, which is set to high values far away from the rigidity transition.

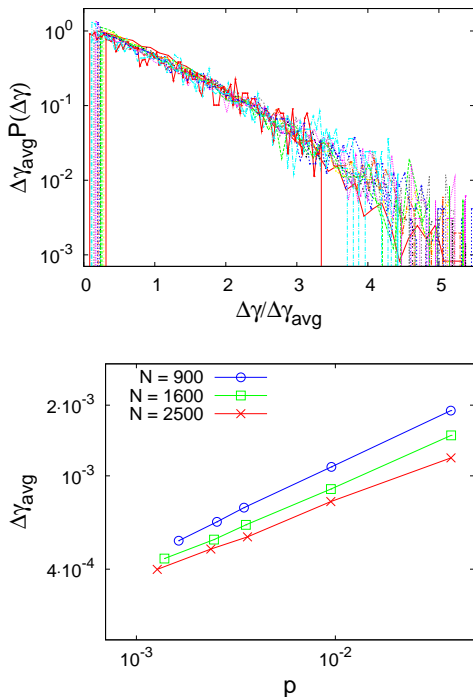


Figure 6: (Top) Distribution of elastic branch length normalized with average values $\Delta\gamma_{\text{avg}}$. (Bottom) Scaling of $\Delta\gamma_{\text{avg}}$ with pressure p . The ratio $g = \Delta\sigma_{\text{avg}}/\Delta\gamma_{\text{avg}}$, which defines a shear-modulus, is consistent with the scaling in Fig. 3.

The authors have argued for a universal value of the “flow-strain” σ_y/g of a few percent. Apparently, this can only be true far away from ϕ_c . As the yield-stress vanishes faster than the shear modulus, one finds a ratio $\sigma_y/g \sim \delta\phi^{1/2}$ that vanishes at point J. Thus, particle configurations at the onset of jamming are highly fragile and susceptible to even minute changes in the boundary conditions.

The average stress-drop as well as the average length of elastic branches change with pressure and system-size as displayed in Figs. 5 and 6². As a function of pressure one observes an increase but with a slope that depends on system-size. The av-

²Note, that these values also depend on the elementary strain step used in the simulations. For any finite step-size there will be some small plastic events, that cannot be resolved but only lead to an apparent reduction of the stress increase. This will artificially increase the length of elastic branches and decrease the weight of the small $\Delta\sigma$ -tail of the stress-drop distribution.

erage stress-drops increase somewhat slower with pressure than the yield-stress³. The relative stress fluctuations $\Delta\sigma_{\text{avg}}/\sigma_y$ are thus slightly enhanced at small pressures close to ϕ_c . The same trend is also visible in the total stress fluctuations as calculated by $\langle(\sigma - \langle\sigma\rangle)^2\rangle$.

The overall scale of both, $\Delta\sigma_{\text{avg}}$ and $\Delta\gamma_{\text{avg}}$, decreases with system-size to give a smooth stress-strain relation in the thermodynamic limit. Previous studies^{8,10,11} have observed a scaling of the stress-drops with $N^{-1/2}$. This includes⁸ a system of harmonically interacting particles, as studied here, but at a rather high pressure. In general, we observe a weaker dependence on system-size, with an effective exponent that increases with pressure. Our data is consistent, however, with the value of 1/2 being the relevant high-pressure limit.

3.2 Dynamical correlations

Let us now turn to the dynamics of the system. In particular we want to characterize dynamic correlations in the motion of particles. While at volume-fractions above ϕ_c the isostaticity length-scale l^* is clearly finite⁴, there is nevertheless a large dynamical length-scale related to the flow arrest. This has, for example, been evidenced in a system of Lennard-Jones particles with dissipative dynamics.¹⁵ We will show below that a similar length-scale occurs in our system of purely repulsively interacting particles, independent of the distance to ϕ_c .

Let us start by presenting the results from the quasistatic simulations. To define a dynamical correlation length we study heterogeneities in the particle mobilities. To this end we use the overlap-function^{43,44}

$$\langle Q(\gamma, a) \rangle = \left\langle \frac{1}{N} \sum_{i=1}^N \exp \left[-\frac{u_{\text{ina}}(\gamma)^2}{2a^2} \right] \right\rangle, \quad (3)$$

of particles undergoing nonaffine displacements u_{ina} during a strain interval of γ ⁵. Particles moving farther than the distance a (“mobile”), have

³ The effective exponents range from 0.8 to 0.9 as compared to an exponent 0.95 for the yield-stress

⁴If we assume for the isostaticity length $l^* = 1/\delta z$, we would have values $l^* \approx 5$ at $\phi = 0.846$ and $l^* \approx 1$ at $\phi = 0.9$ (z -values taken from Fig. 4).

⁵To calculate the overlap function we use the non-affine displacements in the gradient direction (irrespective of the distance to the wall).

$Q \approx 0$, while those that stay within this distance (“immobile”) have $Q \approx 1$.

As a function of strain γ , the average overlap $\langle Q \rangle$ will decay, when particle displacements u_{na} are comparable to the probing length-scale a . The overlap function is similar to the intermediate scattering function with wave-vector $q \sim 1/a$. Thus, a sets the probing length-scale. The decay of $Q(\gamma, a)$ then gives an associated structural relaxation strain, $\gamma^*(a)$, on which particle positions decorrelate.

In the following we are interested in the dynamical heterogeneity of Q and the fluctuations around its average value

$$\chi_4(a, \gamma) = N \left(\langle Q(\gamma, a)^2 \rangle - \langle Q_a(\gamma, a) \rangle^2 \right), \quad (4)$$

which defines the (self-part of the) dynamical susceptibility χ_4 . This is displayed in Fig. 7 as a function of both strain γ and probing length-scale a . For each γ it has a well defined peak (at $a^*(\gamma)$) that parallels the decay of the overlap function $\langle Q \rangle$.³¹

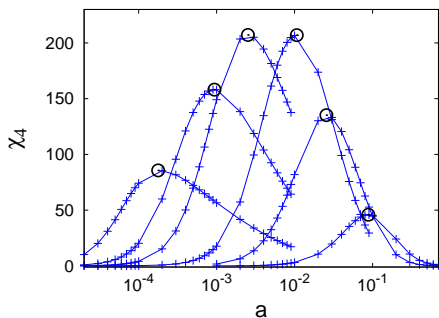


Figure 7: Dynamical susceptibility χ_4 as function of probing length-scale a for various different strains $\gamma = (5, 20, 50, 200, 500, 2000) \cdot 10^{-5}$ (from left to right) and $\phi = 0.9$. The maxima of the curves (black circles) define the amplitude $h(\gamma)$.

The strength of the correlations are encoded in the peak-height, $h(\gamma) \equiv \chi_4(a^*(\gamma), \gamma)$ (black circles in Fig. 7)). As χ_4 can be written as the integral over a correlation function, it is connected to the correlation volume, or to the number of correlated particles. Assuming that this volume forms a compact region in space^{45,46} we can relate the amplitude of χ_4 to a dynamic correlation length via $\xi^2(\gamma) = h(\gamma)$.

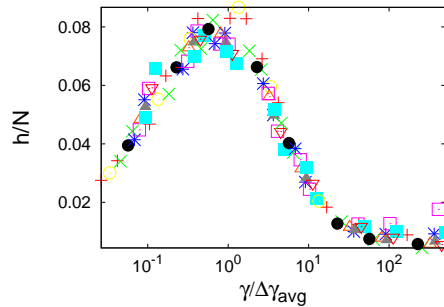


Figure 8: Amplitude $h(\gamma)$ as taken from the quasistatic simulations. Data for different volume-fractions and system-sizes. The axes are normalized according to the scaling form $h(\gamma) = N\tilde{h}(\gamma/\Delta\gamma_{\text{avg}})$, with $\Delta\gamma_{\text{avg}}$ taken from Fig. 6.

Following the maxima in Fig. 7 from left to right, one sees that the amplitude first increases and then quickly drops to small values. This implies that there is a finite strain γ , at which χ_4 presents an *absolute* maximum. To extract this maximum we plot in Fig. 8 the amplitude $h(\gamma)$ for various volume-fractions ϕ and system-sizes N .

There are two surprising features in this plot.

First, by rescaling the strain-axis with the average length of elastic branches, $\Delta\gamma_{\text{avg}}$ (see Fig. 6) we find reasonable scaling collapse for all studied volume-fractions and system-sizes. This implies that cooperativity, as measured by the amplitude of χ_4 and the length of elastic branches are intimately related. The frequency of plastic events sets the strain-scale for dynamical heterogeneities. As the length of the elastic branches decreases with system size, the absolute maximum shifts towards smaller strains, with $h(\gamma)$ becoming effectively a decreasing function of γ in the thermodynamic limit.

The second surprising feature in Fig. 8 is the system-size dependence of h . It turns out that h/N rather than h itself is independent of system-size, indicating a finite variance of the distribution of Q values in the thermodynamic limit (see Eq. (4)). Assuming the connection with the correlation length to hold, $\xi^2 \sim h$, this implies a correlation length that is proportional to the length of the simulation box, $\xi \approx 0.3L$, independent of volume-fraction and distance to point J. This illustrates the fact that quasistatic dynamics is inher-

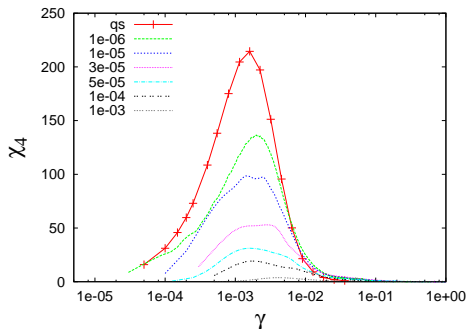


Figure 9: $\chi_4(\gamma)$ for different strain-rates $\dot{\gamma}$ and $a = 0.01$. comparison with quasistatic ('qs') simulations. Note the different boundary conditions used. MD simulations are with walls, while quasistatic simulations have periodic boundary conditions. This may explain the difference in the amplitude.

ently dominated by system-size effects, as already shown in previous works^{14,15,28,47}. Note, that this system-size dependence is of different origin than the finite-size effects present within the above mentioned intermittent regime, which occurs close to ϕ_c . The intermittency can be avoided by staying away from ϕ_c . In contrast, the system-size dependence encountered here is quite independent of volume-fraction, but rather a generic feature of the quasistatic regime, as we show now.

To this end let us turn to the molecular-dynamics simulations. We will show that the dependence on system-size indeed reflects the saturation of a length-scale that is finite for larger strain-rates and increases towards the quasistatic regime⁶. As Fig. 9 shows, the amplitude of χ_4 increases when reducing the strain-rate ($a = 0.01$, $\phi = 0.9$) and approaches the quasistatic limit for small strain-rates. Also the strain γ_m , at which χ_4 is maximal is very well reproduced in the dynamic simulation.

Fig. 10 demonstrates a saturation of the amplitude $\chi_m \equiv \chi_4(\gamma_m)$ at small strain-rates indicating that the quasistatic regime is entered. Comparing with the quasistatic simulation, we find somewhat smaller values for the amplitude. It should be remembered, however, that different boundary con-

⁶A more detailed account of these simulations will be presented in: P. Chaudhuri and L. Bocquet, in preparation (2010).

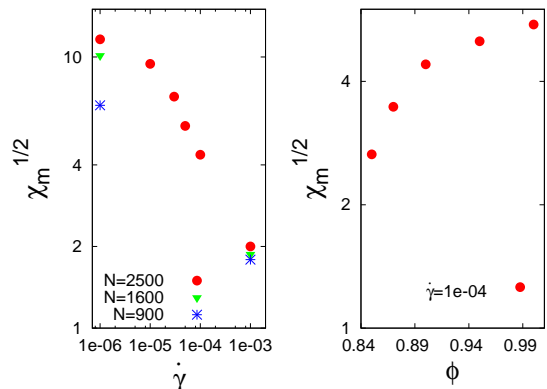


Figure 10: (Left) Peak-height $\chi_m = \chi_4(\gamma_m)$ as determined from Fig. 9. The saturation at small strain-rates is an indication of the quasistatic limit, in which $\chi_m \sim N$. In contrast, at high strain-rates no significant dependence on system-size is observed. (Right) Peak-height χ_m as function of volume-fraction.

ditions have been used. The rough walls used in the molecular dynamics simulations are likely responsible for the reduction of the peak-height as compared to the quasistatic simulations (which are performed with periodic boundary conditions).

The presence of the quasistatic regime is also evidenced by the fact that the amplitude χ_m within the plateau depends on system-size, just as in the quasistatic simulations. Outside this regime, on the other hand, no significant N -dependence is observed. In effect this means that the quasistatic regime shrinks with increasing system-size. The strainrate $\dot{\gamma}_{qs}(N)$ that describes the crossover to the quasistatic regime decreases with N . This is in line with Refs.^{14,15} where a power-law dependence $\dot{\gamma}_{qs} \sim 1/N$ is reported. From our data we cannot make any definitive statement about this dependence.

The results are furthermore consistent with those of Ono *et al.*⁴⁸ The lowest strain-rate accessible in the latter study was $\dot{\gamma} = 0.0001$. At this strain-rate the correlation length was observed to be on the order of 3 in agreement with our data.

We also probed the volume-fraction dependence, by performing runs at $\phi = 0.85, 0.87, 0.9, 0.95$ and 1. The resulting amplitude of χ_4 is given in Fig. 10. Interestingly we observe a mild increase in the am-

plitude with volume-fraction, signalling enhanced correlations *away* from ϕ_c .

This is not due to the special choice of the parameter $a = 0.01$. We have found the same trend when fixing γ and viewing χ_4 as function of a as for the quasistatic simulations in Fig. 7. Finally, we have also calculated the *absolute maximum* of χ_4 , viewed as function of both a and γ . In all cases, the amplitude increases with volume-fraction. Both, the increase of the length-scale with lowering the strain-rate and the increase with volume-fraction are consistent with the recently proposed elasto-plastic model of Bocquet *et al.*¹³

Given the trend in Fig. 10, one may speculate about a vanishing dynamical correlation length (taken at constant strain-rate $\dot{\gamma} = 10^{-4}$ outside the quasistatic regime), as ϕ_c is approached. Such a behavior is indeed compatible with our data and has recently been observed in the rheology of a concentrated emulsion confined in gaps of different thickness.⁴⁹ Here we interpret this surprising feature in the following way: at a given packing fraction, dynamical correlations increase with decreasing $\dot{\gamma}$, and saturate at a N -dependent value in the quasistatic regime. This cross-over to the quasistatic regime does not only depend on system-size but also on packing fraction: $\dot{\gamma}_{\text{qs}}(N, \phi)$.

For ϕ closer to ϕ_c the energy landscape becomes increasingly flat. Particle relaxations take longer⁵⁰ and smaller strain-rates are needed to allow for full relaxation into the local energy minimum. Thus, smaller strain-rates are needed to reach the quasistatic behavior and $\dot{\gamma}_{\text{qs}}$ decreases towards ϕ_c . Hence, reducing ϕ towards ϕ_c *at a fixed strain rate* is "equivalent" to increasing the strain rate relative to $\dot{\gamma}_{\text{qs}}$, and results in a decrease of dynamical correlations. In contrast, correlations taken at a strain rate $\dot{\gamma} = \dot{\gamma}_{\text{qs}}(\phi)$, are independent of ϕ and given by their quasi-static values, as displayed in Fig. 8.

4 Discussion and Conclusion

We have discussed the small strain-rate elasto-plastic flow of an athermal model system of soft harmonic spheres. In particular, we were interested in the flow properties at and above a critical volume-fraction (point J), at which the yield-stress of the material vanishes. This regime combines the more traditional elasto-plastic flow of solids above

their yield-stress with the breakdown of the rigidity of the solid state at point J.

We found that this breakdown is visible in the ensemble of states visited during a flow simulation in a similar way as in the linear elasticity of the solid. For example (Fig. 4), we showed that the average number of particle contacts scale with the square-root of pressure, just as in linear elasticity. In contrast, the fluctuations around this average value show a distinct behavior that has not been observed previously. We showed that the contact-number fluctuations actually diverge upon approaching the critical volume-fraction from above, making the contact number an ideal candidate for an order parameter of a continuous jamming transition as observed under steady shear. The relative fluctuations of the shear modulus and those of the shear stress also diverge in the same limit. Going beyond the characterization of the average elastic properties we have studied the statistics of plastic events (Figs. 5 and 6). It seems that all distributions have universal scaling forms reminiscent of standard critical phenomena.

From all these results, it would be tempting to say that it is the energy landscape as a whole that becomes critical at point J. Isostatic elasticity would then be just one aspect of this criticality, another one could be the intermediate power-law tail in the stress-drop distribution. This critical aspect is also illustrated by the intermittency in the stress response of finite-size systems (see Fig.1) and by the growth of an isostatic correlation length in the quasistatic response when point J is approached from below.²⁸

At strain-rates above the quasistatic regime, the dynamics limits access to certain regions of the energy landscape. While the dynamics is still highly correlated, the dynamical correlation length, as measured by the amplitude of the four-point susceptibility χ_4 , remains finite and actually *decreases* with lowering the volume-fraction towards ϕ_c .

In the quasistatic regime we have shown that χ_4 reflects, in two ways, the interplay of elastic loading and plastic energy release (Fig. 8). First, the typical strain-scale of heterogeneity is set by the frequency of plastic events. Second, the amplitude of χ_4 scales with system-size, which highlights the fact that the quasistatic, plastic flow regime is, in fact, a finite-size dominated regime with a correlation length that is limited by system size. This behavior

should be contrasted with the one observed below ϕ_c , where a large but finite correlation length has been identified, which is governed by the approach to point J.⁵¹

Upon increasing the strain-rate we have shown that the correlation length starts to decrease outside the finite-size scaling regime (Fig. 10). Olsson and Teitel²⁶ infer from their flow simulations that shear-stress should be viewed as a “relevant perturbation” to point J, such that a different fixed-point and indeed different physics is relevant for the flow behaviour at finite stress. Our findings support this picture for the dynamical correlations, which appear to behave similarly to those observed in models of elasto-plastic flow^{13,14,52} or in low temperature glasses:^{10,15} correlations increase upon lowering the strain-rate and saturate at a system-size dependent value in the quasistatic regime.

The flow behaviour in the vicinity of point J is therefore influenced by a complex combination of two critical behaviour. Large stress fluctuations (relative to the yield stress), or geometrical changes (number of neighbours) reflect the enhanced sensitivity of the material to small changes in external conditions at point J, and are specific properties of the energy landscape at this point. On the other hand, dynamical correlations above point J are dominated by the system size, and build up progressively as the strain rate is decreased, as in any elasto-plastic system, and are not particularly sensitive to the proximity of point J.

Acknowledgments The authors acknowledge fruitful discussions with Ludovic Berthier, Lydéric Bocquet, Erwin Frey; Craig Maloney and Michel Tsamados, as well as thank the von-Humboldt Feodor-Lynen, the Marie-Curie Eurosim and the ANR Syscom program for financial support.

References

- [1] A. J. Liu and S. R. Nagel, *Nature*, 1998, **396**, 21.
- [2] M. Dennin, *J. Phys. Cond. Matt.*, 2008, **20**, 283103.
- [3] A. S. Argon, *Acta Metall.*, 1979, **27**, 47.
- [4] A. S. Argon and L. T. Shi, *Acta Metall.*, 1983, **31**, 499.
- [5] M. L. Falk and J. S. Langer, *Phys. Rev. E*, 1998, **57**, 7192.
- [6] E. Bouchbinder, J. S. Langer and I. Procaccia, *Phys. Rev. E*, 2007, **75**, 036107.
- [7] D. L. Malandro and D. J. Lacks, *J. Chem. Phys.*, 1999, **110**, 4593.
- [8] C. E. Maloney and A. Lemaître, *Phys. Rev. E*, 2006, **74**, 016118.
- [9] A. Lemaitre and C. Carol, *Phys. Rev. E*, 2007, **76**, 036104.
- [10] A. Tanguy, F. Leonforte and L.-L. Barrat, *Eur. Phys. J. E*, 2006, **20**, 355.
- [11] M. Tsamados, A. Tanguy, F. Léonforte and J.-L. Barrat, *Eur. Phys. J. E*, 2008, **26**, 283.
- [12] M. Tsamados, A. Tanguy, C. Goldenberg and J.-L. Barrat, *Physical Review E (Statistical, Nonlinear, and Soft Matter Physics)*, 2009, **80**, 026112.
- [13] L. Bocquet, A. Colin and A. Ajdari, *Physical Review Letters*, 2009, **103**, 036001.
- [14] G. Picard, A. Ajdari, F. Lequeux and L. Bocquet, *Phys. Rev. E*, 2005, **71**, 010501(R).
- [15] A. Lemaître and C. Caroli, *Physical Review Letters*, 2009, **103**, 065501.
- [16] C. S. O’Hern, L. E. Silbert, A. J. Liu and S. R. Nagel, *Phys. Rev. E*, 2003, **68**, 11306.
- [17] T. S. Majmudar, M. Sperl, S. Luding and R. P. Behringer, *Phys. Rev. Lett.*, 2007, **98**, 058001.
- [18] J. C. Maxwell, *Philos. Mag.*, 1864, **27**, 27.
- [19] C. R. Calladine, *Int. J. Solids Struct.*, 1978, **14**, 161.
- [20] D. J. Durian, *Phys. Rev. Lett.*, 1995, **75**, 4780–4783.
- [21] M. Wyart, *Ann. Phys. Fr.*, 2005, **30**, 1.
- [22] W. G. Ellenbroek, E. Somfai, M. van Hecke and W. van Saarloos, *Phys. Rev. Lett.*, 2006, **97**, 258001.

- [23] M. Wyart, S. R. Nagel and T. A. Witten, *Europhys. Lett.*, 2005, **72**, 486.
- [24] M. Wyart, L. E. Silbert, S. R. Nagel and T. A. Witten, *Phys. Rev. E*, 2005, **72**, 51306.
- [25] P.-E. Peyneau and J.-N. Roux, *Phys. Rev. E*, 2008, **78**, 011307.
- [26] P. Olsson and S. Teitel, *Phys. Rev. Lett.*, 2007, **99**, 178001.
- [27] T. Hatano, *J. Phys. Soc. Jpn.*, 2008, **77**, 123002.
- [28] C. Heussinger and J.-L. Barrat, *Phys. Rev. Lett.*, 2009, **102**, 218303.
- [29] M. Otsuki and H. Hayakawa, *Physical Review E (Statistical, Nonlinear, and Soft Matter Physics)*, 2009, **80**, 011308.
- [30] N. Xu and C. S. O'Hern, *Phys. Rev. E*, 2006, **73**, 061303.
- [31] F. Lechenault, O. Dauchot, G. Biroli and J.-P. Bouchaud, *Europhys. Lett.*, 2008, **83**, 46002.
- [32] T. K. Haxton and A. J. Liu, *Phys. Rev. Lett.*, 2007, **99**, 195701.
- [33] <http://lammmps.sandia.gov/index.html>.
- [34] <http://prl.aps.org/supplemental/PRL/v102/i21/e218303>.
- [35] P. Chaudhuri, L. Berthier and S. Sastry, arXiv:0910.0364, 2009.
- [36] K. Binder, *Z. Phys. B*, 1981, **43**, 119.
- [37] S. Henkes and B. Chakraborty, *Physical Review E (Statistical, Nonlinear, and Soft Matter Physics)*, 2009, **79**, 061301.
- [38] S. Tewari, D. Schiemann, D. J. Durian, C. M. Knobler, S. A. Langer and A. J. Liu, *Phys. Rev. E*, 1999, **60**, 4385–4396.
- [39] A. Kabla, J. Scheibert and G. Debregas, *J Fluid Mech*, 2007, **587**, 45.
- [40] K. A. Dahmen, Y. Ben-Zion and J. T. Uhl, *Phys. Rev. Lett.*, 2009, **102**, 175501.
- [41] E. Lerner and I. Procaccia, *Physical Review E (Statistical, Nonlinear, and Soft Matter Physics)*, 2009, **79**, 066109.
- [42] N. P. Bailey, J. Schiotz, A. Lemaître and K. W. Jacobsen, *Phys. Rev. Lett.*, 2007, **98**, 095501.
- [43] S. C. Glotzer, V. N. Novikov and T. B. Schröder, *J. Chem. Phys.*, 2000, **112**, 509.
- [44] S. Franz and G. Parisi, *J. Phys. Condens. Matter*, 2000, **12**, 6335.
- [45] O. Dauchot, G. Marty and G. Biroli, *Phys. Rev. Lett.*, 2005, **95**, 265701.
- [46] J. A. Drocco, M. B. Hastings, C. J. Reichhardt and C. Reichhardt, *Phys. Rev. Lett.*, 2005, **95**, 088001.
- [47] C. E. Maloney, *Phys. Rev. Lett.*, 2006, **97**, 035503.
- [48] I. K. Ono, S. Tewari, S. A. Langer and A. J. Liu, *Phys. Rev. E*, 2003, **67**, 061503.
- [49] J. Goyon, A. Colin, G. Ovarlez, A. Ajdari and L. Bocquet, *Nature*, 2008, **454**, 84.
- [50] T. Hatano, *Phys. Rev. E*, 2009, **79**, 050301(R).
- [51] C. Heussinger, L. Berthier and J.-L. Barrat, *Europhys. Lett.*, 2010, **90**, 20005.
- [52] G. Picard, A. Ajdari, F. Lequeux and L. Bocquet, *Eur. Phys. J. E*, 2004, **15**, 371.